1 **Environmental impact and magnitude of paleosol-**

2 **carbonate carbon-isotope excursions marking five**

3 **early Eocene hyperthermals in the Bighorn Basin,**

4 **Wyoming**

5

6 **Hemmo A. Abels[1,*], Vittoria Lauretano[1], Anna E. van Yperen[1,**], Tarek**

7 **Hopman[1,***], James C. Zachos[2], Lucas J. Lourens[1], Philip D. Gingerich[3],**

8 **Gabriel J. Bowen[4]**

9

10 [1] {Department of Earth Sciences, Utrecht University, Budapestlaan 4, 3584 CD,

11   Utrecht, the Netherlands}

12 [2] {Department of Earth and Planetary Sciences, University of California Santa

13   Cruz, 1156 High Street, Santa Cruz, CA 95064, USA}

14 [3] {Department of Earth and Environmental Sciences, University of Michigan, Ann

15   Arbor, Michigan 48109, USA}

16 [4] {Department of Geology and Geophysics, University of Utah, Salt Lake City, UT

17   84112, USA}

18 [*] {now at: Delft University of Technology, Stevinweg 1, 2628 CN, Delft,

19   Netherlands}

20 [**] {now at: University of Olso, Sem Sælands vei 1, Blindern, 0371 Oslo, Norway}

21 [**] {now at: PanTerra, Weversbaan 1-3, 2352 BZ, Leiderdorp, Netherlands}

22 Correspondence to*: Hemmo A. Abels (h.a.abels@tudelft.nl)

23

24

25

Abstract

Transient greenhouse warming events in the Paleocene and Eocene were associated with the addition of isotopically-light carbon to the exogenic atmosphere-ocean carbon system, leading to substantial environmental and biotic change. The magnitude of an accompanying carbon isotope excursion (CIE) can be used to constrain both the sources and amounts of carbon released during an event, and also to correlate marine and terrestrial records with high precision. The Paleocene Eocene Thermal Maximum (PETM) is well documented, but CIE records for the subsequent warming events are still rare, especially from the terrestrial realm.

Here, we provide new paleosol-carbonate CIE records for two of the smaller hyperthermal events, I1 and I2, as well as two additional records of ETM2 and H2 in the Bighorn Basin, Wyoming, USA. Stratigraphic comparison of this expanded, high-resolution terrestrial carbon isotope history to the deep-sea benthic foraminiferal isotope records from ODP Sites 1262 and 1263, Walvis Ridge, in the southern Atlantic Ocean corroborates that the Bighorn Basin fluvial sediments record global atmospheric change. The ~34-m thicknesses of the eccentricity-driven hyperthermals in these archives corroborate precession-forcing of the ~7-m thick fluvial overbank-avulsion sedimentary cycles. Using CALMAG bulk-oxide mean-annual-precipitation reconstructions, we find similar or slightly wetter than background soil moisture contents during the four younger hyperthermals, in contrast to soil drying observed during the PETM using the same proxy, sediments, and plant fossils.

The magnitude of the CIEs in soil carbonate for the four smaller, post-PETM events scale nearly linearly with the equivalent event magnitudes documented in marine records. In contrast, the magnitude of the PETM terrestrial CIE is at least 5‰ smaller than expected based on extrapolation of the scaling relationship established from the smaller events. We evaluate the potential for recently documented, non-linear effects of pCO$_2$ on plant-photosynthetic C-isotope fractionation to explain this scaling discrepancy. We find that the PETM anomaly can be explained only if background pCO$_2$ was at least 50% lower during most of the post-PETM events than prior to the PETM. Although not inconsistent with other pCO$_2$ proxy data for the time interval, this would require declining pCO$_2$ across an interval of global warming. A more

likely explanation of the PETM CIE anomaly in pedogenic carbonate is that other environmental or biogeochemical factors on the terrestrial CIE magnitudes were not similar in nature or proportional to event size across all of the hyperthermals. We suggest that contrasting regional hydroclimatic change between the PETM and subsequent events, in line with our soil proxy records, may have modulated the expression of the global CIEs in the Bighorn Basin soil carbonate records.

1   Introduction

During the late Paleocene and early Eocene around 60 to 50 million years ago massive amounts of carbon were released in pulses into the ocean-atmosphere exogenic carbon pool causing a series of transient global warming events, known as hyperthermals (Kennett and Stott, 1991; Cramer et al. 2003; Zachos et al., 2005; Lourens et al., 2005). These events represent the best paleo-analogs for current greenhouse gas warming, despite the very different background climatic, atmospheric, and geographic conditions, and potentially the different time scales on which they occurred (Bowen et al., 2006; Zachos et al., 2008; Cui et al., 2011; Bowen et al. 2015). The largest of the hyperthermals, the Paleocene-Eocene Thermal Maximum (PETM) at 56 million years ago, is known to have caused severe climatic and marine and terrestrial biotic change (Thomas, 1989; Gingerich, 1989; Kennett and Stott, 1991; Koch et al., 1992), comprehensively reviewed in McInerney and Wing (2011). Recently, records of the secondary hyperthermals (i.e., ETM-2/H1, ETM3/K) became available (Cramer et al. 2003; Lourens et al. 2005; Nicolo et al. 2007; Abels et al. 2012; Chen et al. 2014; Lauretano et al. 2015), while their environmental and biotic impact has yet to be resolved (Sluijs et al., 2009; Stap et al., 2010a,b; Abels et al., 2012; D'Haenens et al. 2014).

All hyperthermals are characterized by a distinct geochemical signature, a negative carbon isotope excursion, indicating that the carbon released to the exogenic carbon pool during these events had a dominant biogenic origin (Dickens et al., 1995). The potential biogenic sources range from plant material to methane. With the carbon isotope excursions, and independent constraints on the mass of carbon release, it should be possible to identify the source. The mass can be constrained by several approaches, for example quantifying ocean acidification, or pCO$_2$ by proxy, either direct (e.g., epsilon p) or indirect (e.g., SST) (Dickens et al., 1997; Dickens, 2000;

93   Bowen et al., 2004; Ridgwell, 2007; Panchuk et al., 2008; Zeebe et al., 2009), though

94   the uncertainty with these approaches is large (Sexton et al., 2011; DeConto et al.,

95   2012; Dickens, 2011). Nevertheless, in theory, if there was a single source of carbon

96   for all CIE, the scaling with mass should be predictable. This requires that, firstly, the

97   exact size of the carbon isotope excursions (CIEs) in the global exogenic carbon pool

98   during hyperthermal events be well constrained and, secondly, the factors that

99   fractionating C-isotopes between the substrate reservoirs and organic and carbonate

100   proxies be well understood (Sluijs and Dickens, 2012).

101

102   Paleosol or pedogenic carbonate is precipitated from CO_2 that stems from respiration

103   of roots and plant litter in the soil and from atmospheric CO_2 diffusing into the soil.

104   Plant CO_2 from C_3 plants is typically fractionated by -16 to -24‰ compared to

105   atmospheric CO_2 (O'Leary, 1988). Paleosol carbonate is a mix of both isotopically-

106   distinct sources, modified by fractionation associated with diffusion, carbonate

107   equilibrium, and calcite precipitation, and therefore registers values between -7 and -

108   11‰ in non-hyperthermal conditions in Paleogene soils covered by C_3 vegetation.

109   Paleosol carbonate records the atmospheric carbon isotope excursions related to the

110   Paleocene-Eocene Thermal Maximum (PETM), though amplified with respect to

111   marine carbonate (Bowen et al., 2004). This amplification has been attributed to

112   increased soil productivity and humidity during the hyperthermal events (Bowen et

113   al., 2004; Bowen and Bowen, 2008), by changing plant communities (Smith et al.,

114   2007), and by higher $p$$CO_2$ (Schubert and Jahren, 2013).

115

116   In a recent study, the carbon isotope anomalies associated with ETM2 and H2 were

117   documented in paleosol carbonate, allowing for comparison of the terrestrial

118   amplification of the CIEs relative to the PETM (Abels et al. 2012). An apparent linear

119   scaling of the marine and terrestrial carbon isotope excursions for the PETM, ETM2

120   and H2 events was invoked to suggest that all three events may have reflected a

121   common mechanism of global change. Interpretation of this signal is complicated,

122   however, by shifting background climate conditions between the events, which are

123   separated by close to 2 million years of gradual greenhouse warming (Zachos et al.,

124   2008; Littler et al., 2014), and by the fact that the observed relationship did not

125   converge on the origin, leaving the carbon isotope scaling associated with smaller

126   events (e.g., I1 and I2) uncertain.

128   Here, we extend the existing record of three hyperthermals from the Bighorn Basin

129   with data documenting two new CIEs (I1 and I2). We further report additional records

130   of the ETM2 and H2 CIEs within the Basin and analyze bulk oxides in thick (>0.75

131   m) soils to reconstruct soil moisture values through these greenhouse-warming events.

132   We compare our records with the new benthic foraminiferal records generated for

133   Ocean Drilling Program Site 1263 at Walvis Ridge, Atlantic Ocean (Lauretano et al.,

134   2015), and a bulk sediment carbon isotope record from ODP Site 1262 (Zachos et al.,

135   2010; Littler et al., 2014), Walvis Ridge, to investigate coeval carbon isotope change

136   and registration of multiple CIEs in the different carbonate proxies. We analyze these

137   records in the context of recently characterized dependence of plant carbon isotope

138   fractionation on atmospheric CO_2 partial pressure (Schubert and Jahren, 2012),

139   including scenarios that allow for changing background conditions across the late

140   Paleocene-Early Eocene.

141

2   Material and Methods

143   Pedogenic carbonate nodules were sampled at 12.5 cm spacing where present after

144   removal of the weathered surface in the West Branch and Creek Star Hill sections

145   located in the McCullough Peaks area of the northern Bighorn Basin, Wyoming

146   (USA; Fig. 1). Sediment samples from soil-B horizons for reconstruction of Mean

147   Annual Precipitation (MAP) are from the same sections and from the Upper Deer

148   Creek section of Abels et al. (2012).

149

150   Micritic parts of the nodules were cleaned and ground to powder, while spar was

151   taken out after crushing the nodule in few pieces. Carbon isotope ratios of carbonate

152   micrite were measured using a SIRA-24 isotope ratio mass spectrometer of VG

153   (vacuum generators) at Utrecht University (Netherlands). Prior to analysis, samples

154   were roasted at 400°C under vacuum before reaction with dehydrated phosphoric acid

155   in a common-bath system for series of 32 samples and 12 standards. Carbon isotope

156   ratios are reported as $\delta^{13}C$ values, where $\delta^{13}C = (R_{sample}/R_{standard} - 1)$, reported in per

157   mil units (‰), and the standard is VPDB. These isotope ratio measurements are

158   normalized based on repeated measurements of in-house powdered carbonate

159   standard (NAXOS) and analytical precision was calculated from inclusion of three

160   IAEA-CO1 standards in every series of 32 samples. Analytical precision is ± 0.1 ‰

161   for $\delta^{13}C$ (1σ), whereas variability within individual paleosols averaged 0.2‰.

162

163   To calculate CIE magnitudes, carbon isotope records are first detrended to exclude the

164   influence of the long term Paleocene to early Eocene trends. The CIE magnitudes are

165   then calculated as the difference between pre-excursion carbon isotope values and

166   excursion values within the core of the main body (Table 2; Supporting Information).

167   Standard errors are calculated using variability in background and excursion values.

168

169   **3**   **Results**

170   **3.1**   **Bighorn Basin**

171   High-resolution pedogenic carbonate carbon isotope records are constructed for the

172   lower Eocene of the Willwood Formation in the McCullough Peaks area, northern

173   Bighorn Basin, Wyoming (USA; Fig. 1). Previous work included the Upper Deer

174   Creek (UDC) section, where the carbon isotope excursions of ETM2 and H2

175   hyperthermal events were located (Abels et al. 2012). Here, we analyze two parallel

176   sections, the Creek Star Hill (CSH) and West Branch (WB) sections, separated by 1 to

177   2 kilometers from the UDC section (Fig. 1). The isotope record is extended upwards

178   in the WB section and downwards in the Deer Creek Amphitheater section (DCA;

179   Abels et al. 2013). We construct a composite stratigraphic section by connecting the

180   four sections via lateral tracing of marker beds in the field, such as the P1 to P8 purple

181   soils in the ETM2-H2 stratigraphic interval (Abels et al., 2012).

182

183   The carbon isotope record of paleosol carbonate of the McCullough Peaks (MCP)

184   composite section shows four carbon isotope excursions (CIEs; Fig. 2). The lower

185   excursions of ~3.8 and ~2.8‰ in magnitude (see methods for CIE magnitude

186   calculation) have previously been related to the ETM2/H1 and H2 events (Abels et

187   al., 2012) and are shown to be similar in the parallel Upper Deer Creek, West Branch,

188   and Creek Star Hill sections. This confirms the presence and regional preservation of

189   these CIEs in the Willwood Formation. The two younger carbon isotope excursions

190   are ~2.4 and ~1.6‰ in magnitude and both located in the West Branch section (Fig.

191   2). These excursions likely relate to the CIEs of the I1 and I2 events that occur in the

192   subsequent 405-kyr eccentricity maximum after ETM2/H1 and H2 (Cramer et al.,
193   2003).

194

195   Besides these CIEs, several intervals show less-well-defined negative carbon isotope
196   excursions of ~0.5–1‰; two below ETM2 at MCP meter levels 95 and 145, two
197   above H2 at meter levels ~260 and ~290, and one above I2 at meter 400. This scale of
198   variability is harder to detect as the carbon isotopes show background variability of
199   ~1‰ (2σ), possibly noise related to local environmental factors. The spacing between
200   the CIEs and the low amplitude variability in the MCP section is on average ~34 m.
201   Bandpass filtering of this scale of variability specifically shows a strong coherent
202   variation through the ETM2 to I2 interval (Fig. 3).

203

204   Precession-forcing of overbank-avulsion lithological cyclicity in the Willwood
205   Formation was recently substantiated with data from the Deer Creek Amphitheater
206   section (Abels et al., 2013). In the DCA section, the cyclicity occurs at a scale of ~7.1
207   meters. In the three sections now covering ETM2-H2, the cyclicity has a very similar
208   average thickness of ~7.1 meters. The precession cyclicity comprises heterolithic
209   sandy intervals showing little pedogenic imprint alternating with mudrock intervals
210   showing intense pedogenesis. In the precession forcing sedimentary synthesis, the
211   heterolithic intervals are related to periods of regional avulsions and rapid
212   sedimentation, while the mudrocks are related to periods of overbank sedimentation
213   when the channel belt had a relatively stable position (Abels et al., 2013). This scale
214   of sedimentary cyclicity is also observed higher in the West Branch section. Average
215   climatic precession cycles in the Eocene last ~20 kyr resulting in ~7.1 meters of
216   sediment. This gives an average sedimentation rate of ~0.35 m/kyr, resulting in ~96
217   kyr for the 34 meter cyclicity observed in the carbon isotope records in the ETM2-I2
218   interval. This is in line with ~100-kyr eccentricity forcing of individual hyperthermals
219   and a 405-kyr eccentricity forcing of the ETM2-H2 and I1-I2 couples.

220

221   We produce mean annual precipitation (MAP) estimates across the ETM2-I2 interval
222   with the CALMAG method that uses bulk oxide ratios in soil-B horizons (Nordt and
223   Driese, 2010). Conservatively the method reconstructs soil moisture contents in these
224   ancient soils. Ideally, soil-B horizons thicker than 1 meter should be used for this

proxy (Adams et al., 2011). We measured all 59 soil-B horizons thicker than 1m, where possible in multiple, parallel sections. In addition, we measure 24 soil-B horizons between 0.5 and 1 m. Our estimates from the 83 individual soils show a stable soil moisture regime in the early Eocene Bighorn Basin with mean annual precipitation estimates of around 1278 mm/yr (2σ 132 mm/yr; Fig. 2). All except one soil-B horizon thicker than 1.25 m fall in this range. Soil-B horizons below 1.25 m thickness occasionally show drier outliers, of which three are below 1000 mm/yr. There are no striking changes during ETM2, H2, I1, or I2 hyperthermal events. The 5 soils that contribute to our ETM2 reconstructions show a potentially slightly enhanced soil moisture contents with reproduced annual rainfall of 1337 (2σ 88 mm/yr), while the 11 soils in H2 show 1267 mm/yr ($\pm$166), not different from reconstructions for background climate states. There are slightly more dry outliers both in as well as just out the hyperthermals, especially H2, but it should noted that these intervals also have denser sampling, because of the replication of data for these intervals in three parallel sections.

3.2   Walvis Ridge

For comparison of time equivalent carbon isotope change, we use existing and new benthic foraminiferal *Nuttallides truempyi* records from Site 1263 (McCarren et al., 2008; Stap et al., 2010a; Lauretano et al., 2015), the shallowest site of Walvis Ridge with a paleodepth of ~1500 meters. For Site 1263, because *N. truempyi* specimens are absent in the main body of the PETM, the benthic record includes data for the infaunal species *Oridorsalis umbonatus,* which is isotopically similar (McCarren et al., 2008). The *O.* umbonatus data cover most of the CIE though no shells were recovered from the lowermost portion of the clay layer. Data for the ETM2-H2 events are from Stap et al. (2010a) and for I1-I2 from Lauretano et al. (2015). Benthic foraminifera are mostly absent within the Elmo clay layer at Site 1263. A compilation of all Walvis Ridge sites shows very similar benthic carbon isotope excursion values for ETM2 (Stap et al., 2010a). Therefore, we use the next shallowest Site 1265 (paleodepth ~1850 m) to cover the missing ETM2 peak excursion values in Site 1263. The data from *N. truempyi* at Site 1263, generated at 5-cm resolution across the I1 and I2 events, show benthic CIEs of 0.88‰ for I1 and 0.73‰ for I2 (Fig. 3).

258   As a framework for correlation, we plot the long, high-resolution bulk carbonate
259   carbon isotope record from ODP Site 1262 (Zachos et al., 2010) and benthic carbon
260   isotope record from ODP Site 1263 (Fig. 3). Site 1262 is the deepest Site from the
261   ODP Leg 208 Walvis Ridge transect with an approximate paleodepth of 3600 meters.
262   Site 1262 carbon isotope record is orbitally tuned (Westerhold et al., 2008) and
263   capture all Eocene CIE, PETM, ETM2, H2, and I1 and I2 events (Zachos et al. 2010;
264   see also Littler et al. 2014), though the PETM is clearly truncated due to dissolution
265   (Zachos et al. 2005).

266

267   **3.3 CIE comparison with fixed background pCO$_2$**

268   The new records show that CIE magnitudes of both the terrestrial and marine records
269   decrease progressively across the 5 hyperthermal events (Fig. 4). For the four smaller
270   events, the pedogenic carbonate and benthic foraminifera record are strongly, linearly
271   correlated (r^2 = 0.97). The data for the larger PETM event, however, deviate strongly
272   from this trend. As described above, it has previously been observed that Eocene
273   hyperthermal pedogenic carbonate CIEs are generally amplified in magnitude relative
274   to their marine counterparts (Bowen et al. 2004; Smith et al. 2007; Schubert and
275   Jahren, 2013). The new data suggest that the mechanisms leading to this amplification
276   were stronger, relative to the size of the event, for the smaller events than for the
277   PETM.

278

279   We evaluate this observation in the context of one mechanism, sensitivity of land
280   plant photosynthetic ^{13}C-discrimination to change in pCO$_2$, which may affect the C-
281   isotope offset between marine and terrestrial substrates differently among events. We
282   conduct two sets of model experiments, adopting a common framework for both
283   based on the assumption that the carbon sources and nature of environmental change
284   during each event were comparable. Although this assumption is likely over-
285   simplistic, it allows us to evaluate the effects of the photosynthetic discrimination
286   mechanism in isolation and directly evaluate its potential contribution to CIE
287   expression in the new terrestrial records. Specifically, we assume that for each event
288   the CIE magnitude in the atmosphere ($D\delta_{a,h}$) is equal to the CIE magnitude in marine
289   (benthic) records. We also assume that peak pCO$_2$ change for each hyperthermal
290   (Dp_h) is a linear function of marine (benthic) CIE magnitude, which is to some extent

9

291   supported by the temperature change derived from $D\delta^{18}O$ scaling with $D\delta^{13}C$ (Stap et

292   al. 2010a; Lauretano et al. 2015), such that

293          $Dp_h = Dp_{PETM} \times D\delta_{a,h} / D\delta_{a,PETM}.$ (1)

294   As a starting point for our analysis, we use C-isotope data from leaf wax lipids that

295   constrain the magnitude of the PETM CIE within Bighorn Basin plants ($D\delta_{p,PETM} \approx$ -

296   4.2‰; Smith et al., 2007). Decomposing the plant CIE into

297          $D\delta_{p,PETM} = D\delta_{a,PETM} - D\Delta_{PETM},$ (2)

298   where Δ is photosynthetic C-isotope discrimination, we solve for the change in

299   discrimination during the PETM (+0.8‰ using the Walvis Ridge benthic data to

300   estimate $D\delta_{a,PETM}$).

301

302   For any background pCO_2 condition prior to the PETM ($p_{bkg,PETM}$) we can calculate

303   plant carbon isotope discrimination ($\Delta_{bkg,PETM}$) using equation 6 of Schubert and

304   Jahren (2012). Adding this value and $D\Delta_{PETM}$ we obtain the value of PETM

305   photosynthetic discrimination, Δ_{PETM}. We then invert the photosynthetic

306   discrimination equation to find the PETM pCO_2 concentration (p_{PETM}) that gives the

307   estimated discrimination:

308          $p_{PETM} = (\Delta_{PETM} \times a / b + \Delta_{PETM} \times c - a \times c) / (a - \Delta_{PETM}),$ (3)

309   where $a = 28.26$, $b = 0.21$, and $c = 25$ are empirically optimized parameter values

310   (Schubert and Jahren, 2012). We calculated values of p_{PETM} and change in PETM

311   pCO_2 (Dp_{PETM}) across a range of assumed background pCO_2 conditions from 250 to

312   3,000 ppmv (Figure given in Appendix B).

313

314   Building from this framework, our first set of model experiments assume an invariant

315   background pCO_2 value across all five events to evaluate whether the non-linear

316   response of changing photosynthetic discrimination to a range of Dp_h magnitudes

317   across the events can explain the non-linear CIE scaling observed in the terrestrial

318   records. Using $p_{bkg,h} = p_{bkg,PETM}$ and the Dp_h values estimated for each event, we

319   calculated $D\Delta_h$ for each event using the previously referenced photosynthetic

320   discrimination equation. We then apply equation 2 to each event to calculate an

321   estimate of $D\delta_p$ for and compare the implied plant CIE magnitude ($CIE_p = 0 - D\delta_p$)

322   with the observed soil carbonate CIEs to evaluate whether these scale proportionally

323   across all 5 events. If change in plant discrimination explains the non-linear scaling of

the paleosol carbonate CIE magnitudes (CIE_c), assuming all other soil/environmental influences scale proportionally with event magnitude, then we expect that for all events;

$$CIE_{c,h} = CIE_{p,h} \times \beta_1 + \beta_o. \tag{4}$$

Nowhere within the range of background pCO_2 values tested here is this the case (Fig. 5), suggesting that changing photosynthetic discrimination in isolation and under the assumption of near-constant background pCO_2 cannot explain the variation in CIE expression in Bighorn Basin soil carbonates. The exercise shows that large changes in absolute background pCO_2 values do not significantly impact the results.

3.4 Impact on CIE magnitudes of variable background pCO_2

For our second set of experiments, we allow background pCO_2 (p_{bkg}) to change across the study interval and evaluate the p_{bkg} conditions required to reconcile the observed pattern of soil carbonate CIE magnitudes with the marine record. Our initial assumptions and estimates of PETM discrimination and pCO_2 change are as described in section 3.3.

Here we assume that equation 4 does describe the relationship between plant and soil carbonate CIEs, and that there are no fixed offset effects (i.e. $\beta_o = 0$, all factors that affect the size of the carbonate CIEs relative to the plant CIEs scale linearly with event size). It follows that the plant CIE magnitude for each event is

$$D\delta_{p,h} = D\delta_{p,PETM} \times D\delta_{c,h} / D\delta_{c,PETM}. \tag{6}$$

We then calculate the change in photosynthetic discrimination for each event as:

$$D\Delta_h = D\delta_{a,h} - D\delta_{p,h} \tag{7}$$

We now have two differences, Dp_h and $D\Delta_h$, for each event. From the photosynthetic discrimination equation, we can write

$$D\Delta_h = \frac{ab(p_{bkg,h}+Dp_h+c)}{a+b(p_{bkg,h}+Dp_h+c)} - \frac{ab(p_{bkg,h}+c)}{a+b(p_{bkg,h}+c)}. \tag{8}$$

This can be rearranged to give:

$$b^2 p_{bkg,h}{}^2 + b(2a + 2bc + bDp_h)p_{bkg,h} =$$

$$a^2 + 2abc + abDp_h + b^2 c(Dp_h + c) - \frac{a^2 bDp_h}{D\Delta_h}, \tag{9}$$

354   a quadratic which can be solved to obtain the background $p\text{CO}_2$ value required for

355   each hyperthermal to give linear scaling between CIE_p and CIE_c across the events (at

356   any prescribed value of $p_{bkg,PETM}$).

357

358   The analysis suggests that the non-linear scaling of the soil carbonate CIEs relative to

359   the marine record can be explained across the entire range of assumed $p_{bkg,PETM}$

360   conditions through changes in photosynthetic ^{13}C-discrimination forced by

361   hyperthermal $p\text{CO}_2$ increase over a varying background $p\text{CO}_2$ conditions (Fig. 6). For

362   any assumed PETM background $p\text{CO}_2$, our results require a $> 50\%$ decrease in

363   background $p\text{CO}_2$ during the ~2 Myr interval separating the PETM and ETM2. The

364   analysis requires sustained, low background $p\text{CO}_2$ which rises gradually across the

365   two subsequent events, before a more abrupt increase prior to the I2 event. Across

366   most of the range of initial conditions evaluated the results require non-hyperthermal

367   background $p\text{CO}_2$ values substantially lower than $p_{bkg,PETM}$ throughout the Early

368   Eocene. The fractional change in $p\text{CO}_2$ required, relative to PETM background

369   conditions, is lower for higher assumed $p_{bkg,PETM}$, but larger absolute changes in $p\text{CO}_2$

370   are required for these cases.

371

372   **4   Discussion**

373   **4.1   Fluvial sedimentary archives of the Bighorn Basin**

374   The presence of five carbon isotope excursions demonstrates that the river floodplain

375   sedimentary successions in the Bighorn Basin firmly record these global atmospheric

376   events. The two new parallel series in the Bighorn Basin confirm the presence of

377   ETM2 and H2 (Abels et al., 2012). The records of the I1 and I2 events represents the

378   first equivalents in fluvial strata. In the terrestrial realm, I1 has been located in coal-

379   seams in the Fushun Basin, China (Chen et al., 2014), while I2 has not yet been

380   recorded in any other terrestrial record.

381

382   The bulk oxide CALMAG proxy data have been proposed to reflect mean annual

383   precipitation (MAP) through its influence on soil mineral weathering and cation

384   leaching (Nordt and Driese, 2010; Adams et al. 2011). Here, we conservatively use

385   the method as a proxy for soil moisture rather than mean annual precipitation. The

386   data indicate no or slight increases in soil moisture during the four early Eocene

387 hyperthermals. This strongly deviates from observations of paleohydrologic change
388 for the PETM in the northern and southern Bighorn Basin, where the same proxy
389 indicates a decrease in soil moisture (Kraus and Riggins, 2007; Kraus et al., 2013),
390 consistent with a soil morphology index (Kraus et al., 2013), and analysis of fossil
391 leaves (Wing et al., 2005; Kraus et al., 2013). This would suggest that the regional
392 climatic and/or environmental response to the PETM differed from the post-PETM
393 hyperthermals.

394

395 Besides precipitation, temperature, vegetation, and sediment type and rates also have
396 a large impact on soil moisture and changes in CALMAG geochemical data should be
397 considered in light of changes in these factors (Kraus et al., 2013). For the four
398 younger hyperthermals, there are no temperature or vegetation data available for the
399 Bighorn Basin, while the impact of sediment type and rates needs to be investigated
400 for all five hyperthermals. In that sense, it thus remains uncertain whether the
401 observed opposite CALMAG changes between PETM and the four post-PETM
402 hyperthermals relate to diametrically opposed precipitation trends or environmental
403 (depositional) trends.

404

405 The precession forcing of the 7-m thick overbank-avulsion sedimentary cycles (Abels
406 et al., 2013) is in line with ~100-kyr and 405-kyr eccentricity forcing of the carbon
407 cycle changes in the ETM2 to I2 stratigraphic interval (Fig. 3). Mudrock intervals
408 with well-developed purple and purple-red paleosols occur predominantly in the
409 eccentricity maxima, while the minima seem to be richer in sand. This could point to
410 a more prolonged relatively stable position of the channel belt on the floodplain,
411 causing less coarse clastic deposition on the floodplains, during eccentricity maxima
412 (Abels et al., 2013). Such an effect could have occurred in combination with or due to
413 more intense pedogenesis under warmer and wetter climates. However, in this
414 interval, the eccentricity-related change is dominated by the hyperthermal events and
415 corroboration of the eccentricity impact is needed from an interval lacking
416 hyperthermals.

417

418 **4.2   Marine-terrestrial correlations**

419 The benthic carbon isotope record of the I1 and I2 events at Site 1263 reveal very
420 similar patterns as in the bulk and benthic carbon isotope record of Site 1262 (Zachos
421 et al. 2010; Littler et al. 2014) at both eccentricity and precession time scales, as was
422 indicated previously for ETM2 and H2 (Stap et al., 2009). These records even capture
423 very detailed features such as the short-term pre-ETM2 and pre-H2 excursions, and a
424 similar pattern in the I2 excursion. These patterns were clearly driven by changes in
425 the carbon isotope ratio of the atmosphere-ocean exogenic carbon pool as related to
426 precession forcing (Stap et al, 2009).

427

428 Some of these precession-scale details are also captured by the pedogenic carbonate
429 carbon isotope record from the Bighorn Basin suggesting their global nature (Fig. 3).
430 A pre-ETM2 excursion occurs in the McCullough Peaks composite at meter 183,
431 while the shape of the I2 excursion is remarkably similar to the marine records. Main
432 differences on these depth scale plots are the relative expanded CIE intervals and
433 short recovery phases between H1 and H2 and between I1 and I2 in the Bighorn Basin
434 with respect to the Atlantic Ocean records. Sediment accumulation rates were
435 influenced by carbonate dissolution in the events and carbonate overshoot after the
436 events in the marine realm. At the same time, in the Bighorn Basin sedimentation
437 rates might have been higher during the events due to increased sediment budgets and
438 subsequently lower during their recovery phases. These processes might cause the
439 expanded CIEs and contracted recovery phases in the Bighorn Basin with respect to
440 the marine records when comparing on depth scale.

441

442 **4.3 Pedogenic carbon isotope excursions**

443 Deciphering the true scale and timing of ocean-atmosphere $\Delta\delta^{13}C$ during
444 hyperthermal events is hampered by environmental impacts on carbon isotope
445 fractionation between marine and terrestrial substrates and their proxies (Sluijs and
446 Dickens, 2012). Our comparison of pedogenic carbonate and marine carbon isotope
447 excursions across the five hyperthermal events shows that although each of the CIEs
448 is amplified in magnitude in the soil carbonate records, the PETM soil carbonate CIE
449 magnitude is anomalously small relative to the pattern of amplification seen for the
450 other events. Changes in photosynthetic ^{13}C-discrimination alone cannot explain the
451 anomalously small PETM soil carbonate CIE if we assume that background $p\mathrm{CO_2}$

452   conditions were similar across each of the events (Fig. 5). This mechanism can

453   explain the soil carbonate CIE scaling across the events if there were substantial

454   changes in background pCO_2, but the required changes involve a $> 50\%$ decline in

455   pCO_2 from the end of the Paleocene to the Early Eocene. This pattern is not

456   inconsistent with independent pCO_2 proxy data from this time interval, but the

457   existing records are too variable and imprecise to provide clear support for or

458   conclusively refute our result (Jagniecki et al. 2015).

459

460   Reconciling the pattern of pCO_2 change inferred in our analysis with known changes

461   in global climate of the early Eocene is more challenging. The dramatic reduction in

462   pCO_2 we estimate following the PETM would be expected to align with a decrease in

463   global temperatures. Although transient cooling has been documented during the ~2

464   Myr following the PETM (Wing et al., 1999), temperatures had recovered to at least

465   pre-PETM levels by the time of the ETM2, and thereafter continued to warm toward

466   the peak Cenozoic values of the Early Eocene Climate Optimum (Zachos et al. 2008).

467   Benthic oxygen isotope data of Walvis Ridge, Atlantic Ocean, show a ~1$°$C increase

468   of deep-sea temperature between PETM and ETM2 baseline values (Littler et al.,

469   2014). The substantially lower background pCO_2 values required by our analysis for

470   ETM2 and the subsequent hyperthermals would thus imply that non-CO_2 greenhouse

471   gases or other mechanisms drove long-term global climatic change during the Early

472   Eocene. This is one possible reading of the record of terrestrial CIE amplification

473   across Early Eocene hyperthermals, and suggests that this record may embed valuable

474   information on long-term changes in atmospheric pCO_2, but it is necessary to

475   acknowledge that the interpretations derived here assume that other local,

476   environmental influences on the terrestrial CIE magnitudes were similar in nature and

477   proportional to event size across all of the hyperthermals.

478

479   Many other factors may potentially modulate the expression of the global

480   hyperthermal CIEs in the Bighorn Basin pedogenic carbonate records, including

481   changes in temperature effects on carbon isotope fractionation, changes in mixing

482   ratios of atmospheric and organic-derived CO_2 in soils, and changes in vegetation

483   composition (Bowen et al., 2004; Smith et al., 2007). If each of these factors

484   responded primarily to CO_2-driven hyperthermal global change then it is reasonable

to assume a proportional, though perhaps non-linear, magnitude of effect across the suite of events. Our data, however, suggest at least one potential forcing factor for these effects, soil moisture, changed in a fundamentally different way during the PETM than during the four younger and smaller hyperthermals (Fig. 2). There is clear indication of soil drying during the PETM based soil development and chemical proxies in line with plant results (Kraus and Riggins, 2007; Kraus et al. 2013). The data presented here for the subsequent ETM2-I2 events show unchanged or slightly increased soil moisture levels.

Soil moisture, likely reflecting more general changes in local hydroclimate, would be expected to influence the soil carbonate CIE records through changes in gas-phase permeability of the soil matrix (with wetter soils trapping more organic-derived CO_2, leading to lower carbonate $\delta^{13}C$ values), influences on ecosystem productivity (with wetter soils supporting higher productivity, soil respiration, and lower $\delta^{13}C_c$), and changes in plant photosynthetic discrimination (with greater soil water availability increasing discrimination and reducing $\delta^{13}C_c$; Kohn et al. 2010; Diefendorf et al. 2010). Soil moisture differences between the PETM and younger hyperthermals could also have led to distinct plant community changes affecting the respective CIEs in pedogenic carbonate (Smith et al. 2007).

Evaluating just one of these potential changes, the reconstructed shift in precipitation inferred from PETM proxy data (a reduction in mean annual precipitation from ~1400 mm/year to ~900 mm/year; Kraus et al. 2013; this study) would, based on data documenting modern relationships between precipitation and photosynthetic discrimination (Kohn et al. 2010; Diefendorf et al. 2010), equate to a reduction in plant discrimination (and thus $CIE_{c,PETM}$) of ~0.9 to ~1.2‰. Our data suggest that changes in precipitation were negligible during the younger hyperthermals, thus this effect could explain ~1‰ of the observed 5‰ PETM CIE_c anomaly. Clearly this points to the need for a more comprehensive analysis including the effects of discordant local environmental changes on the expression of the global hyperthermal CIEs in soil carbonate records, but it also suggests that in many cases these effect sizes may be modest relative to those arising from pCO_2-driven changes in photosynthetic discrimination.

5   Conclusions

We recovered carbon isotope excursions of 2.4 and 1.6‰ respectively related to the I1 and I2 events in floodplain sedimentary records from the Bighorn Basin, Wyoming. This adds to the three earlier found CIEs, the PETM, ETM2, and H2, underlining the sensitivity of these floodplain records for recording global atmospheric changes. Correlations with marine records and eccentricity-forcing of hyperthermals corroborate the continuity of sedimentation that occurred in the basin starting above precession time scales of ~20 kyr. The 35-m short eccentricity-driven hyperthermal events are in line with precession forcing of the 7-m overbank-avulsion sedimentary cycles. Our CALMAG proxy-based soil moisture estimates reproduce similar or slightly enhanced soil moisture contents for the younger four hyperthermals, in contrast to reconstructions for the PETM. More environmental reconstructions, such as from vegetation, are needed for these four younger hyperthermals in the Bighorn Basin to confirm such a remarkable difference.

We find that the magnitudes of Bighorn Basin soil carbonate CIEs are linearly proportional to those recorded in benthic marine records for the post-PETM hyperthermals, but that the soil carbonate CIE for the PETM is ~5‰ smaller than expected based on extrapolation of the relationship observed for the other events. We show that the recently characterized dependence of photosynthetic ^{13}C-discrimination on atmospheric pCO_2 could explain this PETM excursion magnitude 'anomaly', but would require substantially lower background (non-hyperthermal) pCO_2 conditions in the Early Eocene than at the Paleocene-Eocene boundary. That would require reconciliation with globally increasing temperatures during this time interval. Local environmental effects, such as the proxy-inferred reduction of mean annual precipitation during the PETM, likely also modulated the expression of the global hyperthermal CIEs in the Bighorn Basin soil carbonate records. The record of terrestrial carbonate CIE amplification across the sequence of hyperthermals may embed information on million-year changes in early Eocene pCO_2. However, more like, it records the influence of non-uniform local/regional environmental responses to these events, perhaps reflecting the crossing of discrete climate system or ecological thresholds during the PETM that were not reached during the smaller, subsequent hyperthermals.

552

Appendix A.

Carbon isotope and soil bulk oxide results for the McCullough Peaks composite
section.

556

Appendix B.

Figure showing p_{PETM} and change in PETM pCO_2 (Dp_{PETM}) across a range of assumed
background pCO_2 conditions from 250 to 3,000 ppmv.

560

Acknowledgements

570

571

References

Abels, H.A., W.C. Clyde, P.D. Gingerich, F.J. Hilgen, H.C. Fricke, G.J. Bowen, and
    L.J. Lourens: Terrestrial carbon isotope excursions and biotic change during
    Palaeogene hyperthermals. Nature Geosci. 5, 326-329, 2012.

Abels, H.A., M.J. Kraus, and P.D. Gingerich: Precession-scale cyclicity in the fluvial
    lower Eocene Willwood Formation of the Bighorn Basin, Wyoming (USA).
    Sedimentology, doi 10.1111/sed.12039, 2013.

Adams, J.S., M.J. Kraus, and S.L. Wing: Evaluating the use of weathering indices for
    determining mean annual precipitation in the ancient stratigraphic record.
    Palaeogeogr., Palaeocl., Palaeoecol. 309, 358-366, 2011.

582 Bowen, G. J., Beerling, D. J., Koch, P. L., Zachos, J. C., and Quattlebaum, T.: A
583 humid climate state during the Paleocene-Eocene Thermal Maximum. Nature 432,
584 495-499, 2004.

585 Bowen, G. J., Koch, P. L., Gingerich, P. D., Norris, R. D., Bains, S. and Corfield, R.
586 M.: Refined isotope stratigraphy across the continental Paleocene-Eocene
587 boundary on Polecat Bench in the Northern Bighorn Basin *in* Paleocene-Eocene
588 stratigraphy and biotic change in the Bighorn and Clark Fork Basins, Wyoming (ed
589 Gingerich, P.D.) 73-88 (University of Michigan Papers on Paleontology 33,
590 http://hdl.handle.net/2027.42/48328), 2001.

591 Bowen, G.J.: Up in smoke: A role for organic carbon feedbacks in Paleogene
592 hyperthermals. Global and Planetary Change, 109: 18-29, 2013.

593 Bowen, G.J., B.J. Maibauer, M.J. Kraus, U. Röhl, T. Westerhold, A. Steimke, P.D.
594 Gingerich, S.L. Wing, and W.C. Clyde: Two massive, rapid releases of carbon
595 during the onset of the Palaeocene-Eocene thermal maximum. Nature Geosci. 8,
596 44-47, 2015.

597 Chen, Z., Z. Ding, Z. Tang, X. Wang, and S. Yang: Early Eocene carbon isotope
598 excursions: evidence from the terrestrial coal seam in the Fushun Basin, Northeast
599 China. Geophys. Res. Lett. 41, 3559–3564, doi:10.1002/2014GL059808, 2014.

600 Cramer, B.S., J.D. Wright, D.V. Kent, and M.-P. Aubry: Orbital climate forcing of
601 $d^{13}C$ excursions in the late Paleocene-early Eocene (chrons C24n-C25n).
602 Paleoceanography 18, 4, 1097, 2003.

603 Cui, Y., L.R. Kump, A.J. Ridgwell, A.J. Charles, C.K. Junium, A.F. Diefendorf, K.H.
604 Freeman, N.M. Urban, and I.C. Harding: Slow release of fossil carbon during the
605 Palaeocene-Eocene Thermal Maximum. Nature Geosci. 4, 481-485, 2011.

606 D'Haenens, S., A. Bornemann, P. Claeys, U. Röhl, E. Steurbaut, R.P. Speijer: A
607 transient deep-sea circulation switch during Eocene Thermal Maximum 2.
608 Paleoceanography 29, 370-388, 2014.

609 Dickens, G.R, J.R. O'Neil, D.K. Rea, and R.M. Owen: Dissociation of oceanic
610 methane hydrate as a cause of the carbon isotope excursion at the end of the
611 Paleocene. Paleoceanography 10, 965-971, 1995.

612 Dickens, G.R., M.M. Castillo, J.C. Walker: A blast of gas in the latest Paleocene:
613 Simulating first-order effects of massive dissocation of oceanic methane hydrate.
614 Geology 25, 259-262, 1997.

615   Dickens, G.R.: Methane oxidation during the late Palaeocene thermal maximum.
616   Bull.Soc.Geol.France 171, 37-49, 2000.

617   Diefendorf, A.F., K.E. Mueller, S.L. Wing, P.L. Koch, and K.H. Freeman: Global
618   patterns in leaf 13C discrimination and implications for studies of past and future
619   climate. Proc. Nat. Acad. Sciences 107, 5738-5743, 2010.

620   Gingerich, P. D: New earliest Wasatchian mammalian fauna from the Eocene of
621   northwestern Wyoming: composition and diversity in a rarely sampled high-
622   floodplain assemblage. University of Michigan Papers on Paleontology, 28: 1-97,
623   1989.

624   Hancock, H. J. L., Dickens, G. R., Strong, C. P., Hollis, C. J. & Field, B. D.:
625   Foraminiferal and carbon isotope stratigraphy through the Paleocene-Eocene
626   transition at Dee Stream, Marlborough, New Zealand. New Zealand Journ.
627   Geology Geophys. 46, 1–19, 2003.

628   Hollis, C. J., Dickens, G. R., Field, B. D., Jones, C. M. & Strong, C. P.: The
629   Paleocene-Eocene transition at Mead Stream, New Zealand: a southern Pacific
630   record of early Cenozoic global change. Palaeogeogr., Palaeocl., Palaeoecol. 215,
631   313-343, 2005.

632   Jagniecki, E.A., T.K. Lowenstein, D.M. Jenkins & R.V. Demicco: Eocene
633   atmospheric CO_2 from the nahcolite proxy. Geology 43, 1075-1078, 2015.

634   Kiehl J.T., C.A. Shields: Sensitivity of the Palaeocene–Eocene Thermal Maximum
635   climate to cloud properties. Phil. Trans. R. Soc. A 371, 20130093, 2013.

636   Kirtland Turner, S. & A. Ridgwell: Recovering the true size of an Eocene
637   hyperthermal from the marine sedimentary record. Paleoceanography 28, 1-13.
638   Doi. 10.1002/2013PA002541, 2013.

639   Kraus, M.J., F.A. McInerney, S.L. Wing, R. Secord, A.A. Baczynski, and J.I. Bloch:
640   Paleohydrologic response to continental warming during the Paleocene-Eocene
641   Thermal Maximum, Bighorn Basin, Wyoming. Palaeogeogr., Palaeocl.,
642   Palaeoecol. 370, 196-208, 2013

643   Kraus, M.J. and S. Riggins: Transient drying during the Paleocene-Eocene Thermal
644   Maximum (PETM): Analysis of paleosols in the bighorn basin, Wyoming.
645   Palaeogeogr., Palaeocl., Palaeoecol. 245, 444-461, 2007.

646   Lauretano, V., K. Littler, M. Polling, J.C. Zachos, and L.J. Lourens: Frequency,
647   magnitude and character of hyperthermal events at the onset of the Early Eocene
648   Climatic Optimum. Climate of the Past Discussions, in preparation.

649 Littler, K., U. Röhl, T. Westerhold, and J.C. Zachos: A high-resolution benthic stable-
650   isotope record for the South Atlantic: Implications for orbital-scale changes in Late
651   Paleocene–Early Eocene climate and carbon cycling. Earth Planet. Sci. Letters
652   401, 18-30, 2014.

653 Lourens, L. J., Sluijs, A., Kroon, D., Zachos, J. C., Thomas, E., Röhl, U., Bowles, J.,
654   and Raffi, I.: Astronomical pacing of late Palaeocene to early Eocene global
655   warming events. Nature 435, 1083-1087, 2005.

656 McCarren, H., Thomas, E., Hasegawa, T., Röhl, U., and Zachos, J. C.: Depth
657   dependency of the Paleocene–Eocene carbon isotope excursion: Paired benthic and
658   terrestrial biomarker records (Ocean Drilling Program Leg 208, Walvis Ridge).
659   *Geochemistry, Geophysics, Geosystems* 9, Q10008, doi: 10.1029/2008GC002116,
660   2008.

661 McInerney, F.A. and S.L. Wing: The Paleocene-Eocene Thermal Maximum: A
662   pertuarbation of carbon cycle, climate, and biosphere with implications for the
663   future. Annu. Rev. Earth Planet. Sci. 39, 489-516, 2011.

664 Meissner, K.J., T.J. Bralower, K. Alexander, T. Dunkley Jones, W. Sijp, and Ward,
665   M.: The Paleocene-Eocene Thermal Maximum: How much carbon is enough?
666   Paleoceanography 29, 946-963, 2014.

667 Nicolo, M. J., Dickens, G. R., Hollis, C. J. and Zachos, J. C.: Multiple early Eocene
668   hyperthermals: their sedimentary expression on the New Zealand continental
669   margin and in the deep sea. Geology 35, 699–702, 2007.

670 O'Leary, M.H.: Carbon isotopes in photosynthesis. Bioscience, 38: 328-336, 1988.

671 Schouten, S., M. Woltering, W. I. C. Rijpstra, A. Sluijs, H. Brinkhuis, and J. S.
672   Sinninghe Damsté: The Paleocene–Eocene carbon isotope excursion in higher
673   plant organic matter: Differential fractionation of angiosperms and conifers in the
674   Arctic. Earth Planet. Sci. Lett. 258(3-4), 581–592, 2007.

675 Schubert, B.A. and A.H. Jahren: The effect of atmospheric CO_2 concentration on
676   carbon isotope fractionation in C3 land plants. Geochimica et Cosmochimica Acta
677   96, 29-43, 2012.

678 Schubert, B.A. and A.H. Jahren: Reconciliation of marine and terrestrial carbon
679   isotope excursions based on changing atmospheric CO_2 levels. Nature
680   Communications 4: 1653, doi: 10.1038/ncomms2659, 2013.

681   Sexton, P.F., R.D. Norris, P.A. Wilson, H. Pälike, T. Westerhold, U. Röhl, C.T.

682   Bolton, and S. Gibbs. Eocene global warming events driven by ventilation of

683   oceanic dissolved organic carbon. Nature 471, 349-353, 2011.

684   Sluijs, A. and G.R. Dickens: Assessing offsets between the d13C of sedimentary

685   components and the global exogenic carbon pool across early Paleogene carbon

686   cycle perturbations. Glob. Biogeochem. Cycles 26, GB4005, doi.

687   10.1029/2011GB004224, 2012.

688   Smith, F.A., S.L. Wing, K.H. Freeman: Magnitude of the carbon isotope excursion at

689   the Paleocene-Eocene thermal maximum: the role of plant community change.

690   Earth Planet. Sci. Lett. 262, 50-65, 2007.

691   Stap, L., Sluijs, A., Thomas, E., and Lourens, L. J.: Patterns and magnitude of deep

692   sea carbonate dissolution during Eocene Thermal Maximum 2 and H2, Walvis

693   Ridge, southeastern Atlantic Ocean: Paleoceanography 24, PA1211, doi:

694   10.1029/2008PA001655, 2009.

695   Stap, L., Lourens, L. J., Thomas, E., Sluijs, A., Bohaty, S., and Zachos, J. C.: High-

696   resolution deep-sea carbon and oxygen isotope records of Eocene Thermal

697   Maximum 2 and H2. Geology 38, 607-610, 2010a.

698   Stap, L., L. Lourens, A. van Dijk, S. Schouten, & E. Thomas: Coherent pattern and

699   timing of the carbon isotope excursion and warming during Eocene Thermal

700   Maximum 2 as recorded in planktic and benthic foraminifera. Geochemistry,

701   Geophysics, Geosystems 11, Q11011, doi. 10.1029/2010GC003097, 2010b.

702   Thomas, E.: Development of Cenozoic deep-sea benthic foraminiferal faunas in

703   Antarctic waters. In J. A. Crame (ed.), Origins and Evolution of the Antarctic

704   Biota, Geological Society Special Publication, 18: 283-296, 1989.

705   Uchikawa, J., & R.E. Zeebe: Examining possible effects of seawater pH decline on

706   foraminiferal stable isotopes during the Paleocene-Eocene Thermal Maximum.

707   Paleoceanography 25, PA2216, doi. 10.1029/2009PA001864, 2010.

708   Wing, S.L., Bao, H., Koch, P.L.: An early Eocene cool period? Evidence for

709   continental cooling during the warmest part of the Cenozoic. In: Huber, B.T.,

710   Macleod, K.G., Wing, S.L. (Eds.), Warm Climates in Earth History. Cambridge

711   University Press, Cambridge, UK, pp. 197-237, 1999.

712   Zachos, J.C., U. Röhl, S.A. Schellenberg, A. Sluijs, D.A. Hodell, D.C. Kelly, E.

713   Thomas, M. Nicolo, I. Raffi, L.J. Lourens, H. McCarren, and D. Kroon: Rapid

714   acidification of the ocean during the Paleocene-Eocene Thermal Maximum.

715   Science 308, 1611-1615, 2005.

716   Zachos, J.C., S.M. Bohaty, C.M. John, H. McCarren, D.C. Kelly, and T. Nielsen: The

717   Palaeocene-Eocene carbon isotope excursion: constraints from individual shell

718   planktonic foraminifer records. Phil. Trans. R. Soc. A 365, doi.

719   10.1098/rsta.2007.2045, 2007.

720   Zachos, J. C., Dickens, G. R. & Zeebe, R. E.: An early Cenozoic perspective on

721   greenhouse warming and carbon-cycle dynamics. Nature 451, 279-283, 2008.

722   Zeebe, R.E., Zachos, J.C., Dickens, G.R.: Carbon dioxide forcing alone insufficient to

723   explain Palaeocene-Eocene Thermal Maximum warming. Nature Geosci., 2: 576-

724   580, 2009

725

726   **Tables**

727   Table 1. Nomenclature.

a	atmosphere
bkg	background
CIE	carbon isotope excursion
CIE_c	CIE in paleosol carbonate
D	difference
$D\delta$	carbon isotope excursion magnitude
Δ	photosynthetic C-isotope discrimination
h	non-PETM hyperthermal
p	pCO_2
pCO_2	atmospheric CO_2 pressure
PETM	Paleocene Eocene Thermal Maximum

728

729

730   Table 2. Magnitudes of carbon isotope excursions for five Paleocene-Eocene

731   hyperthermal events in paleosol carbonate of the Bighorn Basin, Wyoming (USA)

732   and benthic foraminiferal and bulk sediment carbonate of Walvis Ridge Sites 1263

733   and 1262, Atlantic Ocean. Standard errors of the differences between detrended

734   background variability and excursion variability are given (see Methods).

Event	Bighorn Basin CIE ped.carb.	st.error	Bighorn Basin CIE n-alkanes	st.error	Walvis Ridge Sites 1263/65 CIE ben.forams	st.error	Walvis Ridge Site 1262 CIE bulk carb.	st.error
PETM	**5.90**	0.86	**4.23**	0.67	**3.38**	0.12	**1.93**	0.08
EMT2 / H1	**3.78**	0.56			**1.30**	0.18	**0.89**	0.05
H2	**2.75**	0.38			**0.97**	0.16	**0.58**	0.06
I1	**2.42**	0.45			**0.88**	0.16	**0.63**	0.07
I2	**1.55**	0.72			**0.73**	0.16	**0.50**	0.10

735

Figures

738

739 Figure 1. Location map of the sampling sites in the McCullough Peaks area of the
740   northern Bighorn Basin in northeastern Wyoming (USA). Background colors
741   denote topography, grey lines are roads. Indicated are the fossil localities and their
742   interpreted Wasatchian mammal zone and the four study sections. Polecat Bench in
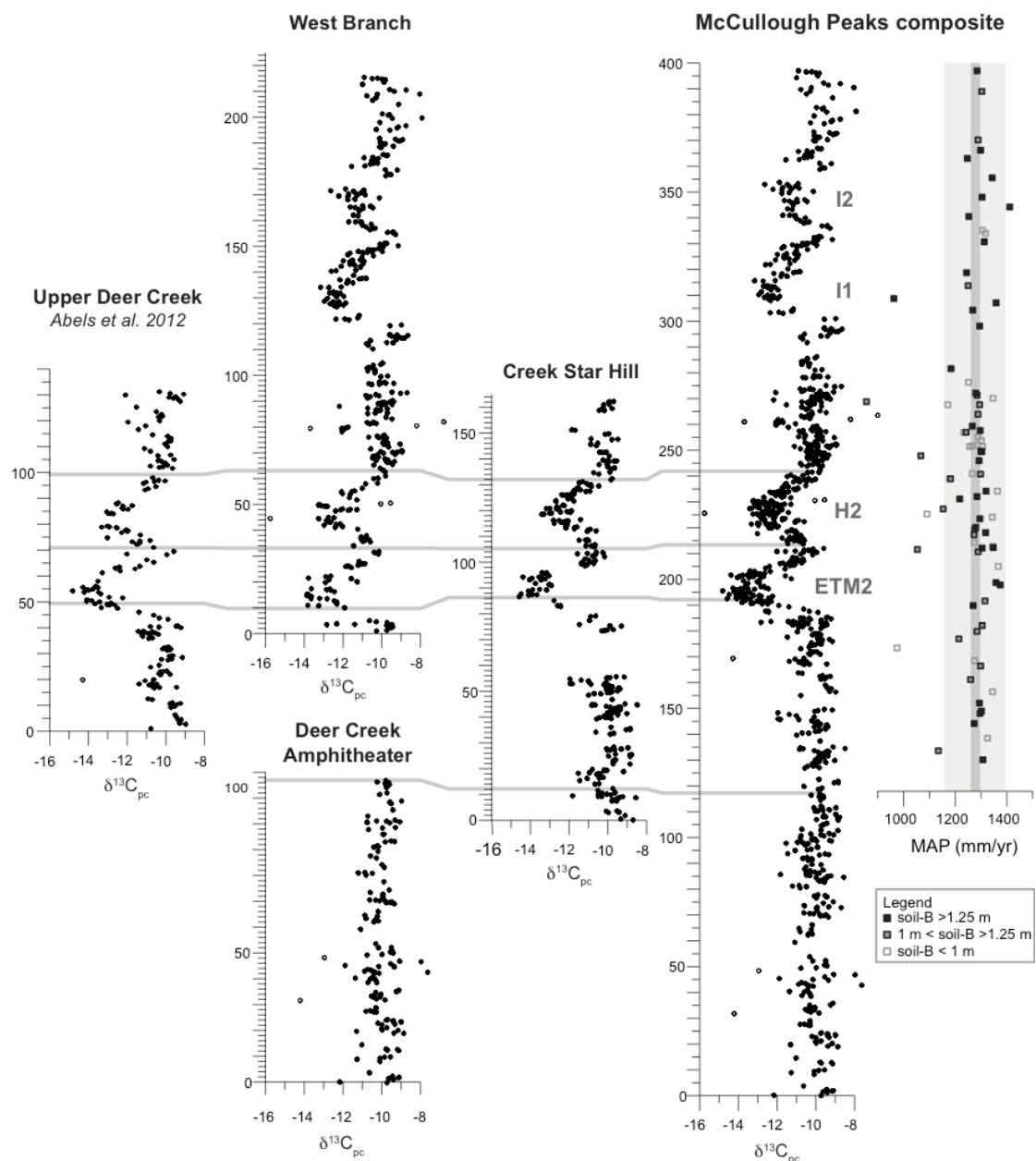743   the northwest of the study sites is the location of the PETM.

744

Figure 2. Carbon isotope stratigraphies of paleosol carbonate in the McCullough
Peaks area, Bighorn Basin, Wyoming (USA). Shown are data from the Upper Deer
Creek section of Abels et al. (2012), and the West Branch, Deer Creek
Amphitheater, and Creek Star Hill sections. Grey horizontal lines represent field-
based tracing of marker beds P1, P4, and P8 by which the McCullough Peaks
composite carbon isotope stratigraphy has been constructed. To the right, Mean
Annual Precipitation reconstructions from the CALMAG methods are given on the
McCullough Peaks composite stratigraphy. Different symbols denote different
thickness of the soil-B horizons. Note that there is no obvious change in soil
moisture during the four hyperthermal events.
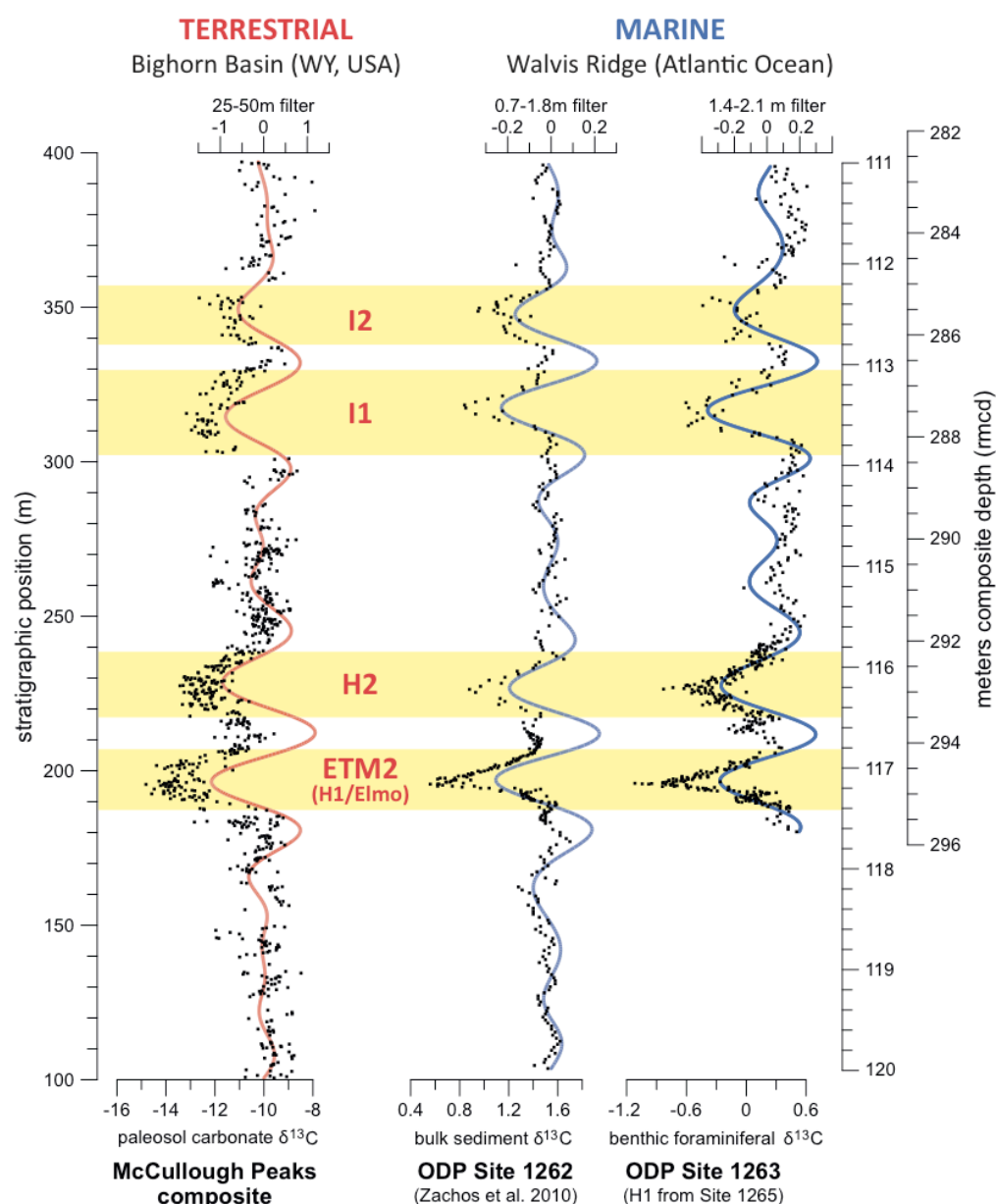
Figure 3. The McCullough Peaks paleosol carbonate carbon isotope stratigraphy compared in depth domain to the bulk sediment and benthic foraminiferal (*Nutallides truempyi*) carbon isotope stratigraphies at, respectively, ODP Site 1262 (left y-axis on right side; Zachos et al., 2010) and 1263 (right y-axis on right side; Stap et al. 2010a; this study) at Walvis Ridge in the southern Atlantic Ocean. Filters denote the ~100-kyr eccentricity band in the three records. Note that linear stretching of depth scales is sufficient to construct the figure indicating the constant average sedimentation rates at longer time scales in both realms. At smaller time scales, large sedimentation rate differences occur that in the marine realm relate to carbonate dissolution during and carbonate overshoot after the hyperthermal events.
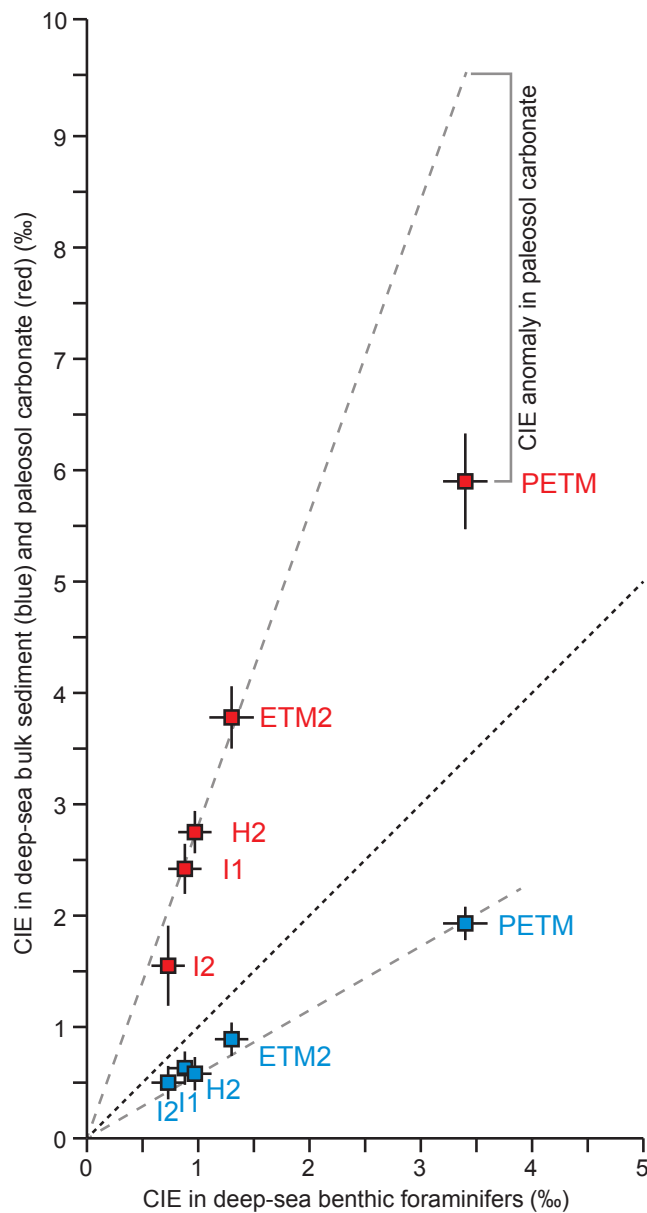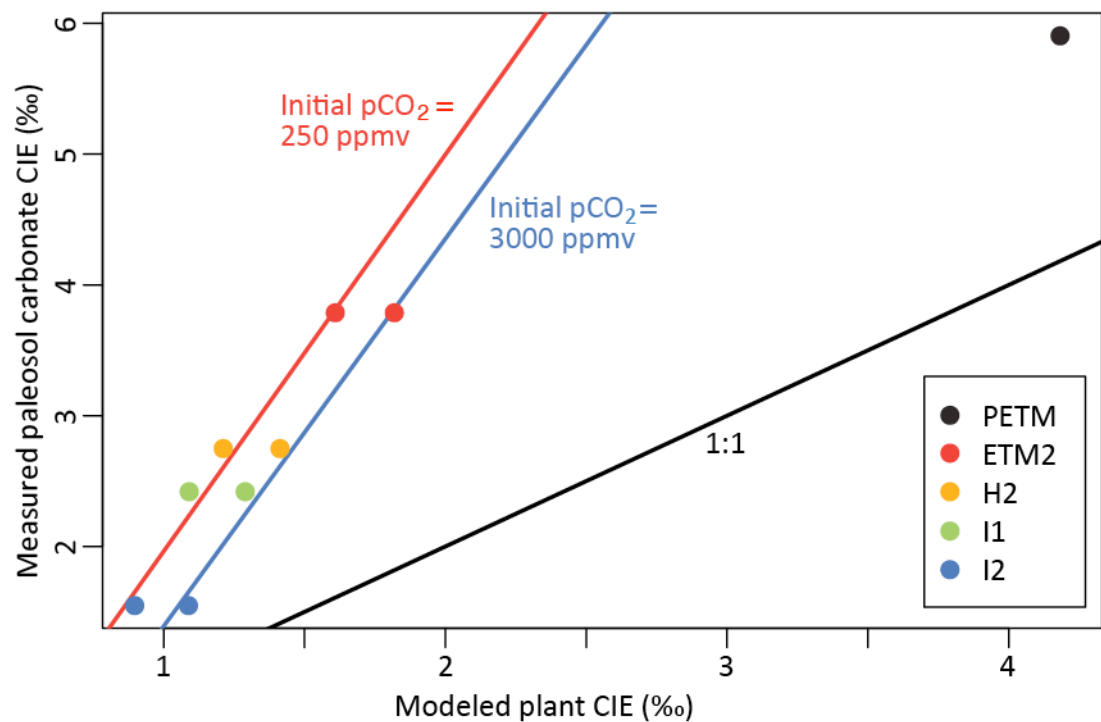
767

768　　Figure 4. Carbon isotope excursions (CIEs) for the PETM, ETM2, H2, I1, and I2

769　　　　events in the early Eocene compared between different proxies in marine and

770　　　　terrestrial settings. Blue squares denote benthic foraminiferal (x-axis) versus bulk

771　　　　sediment (y-axis) CIEs at Walvis Ridge in the Atlantic Ocean. Red squares denote

772　　　　benthic foraminiferal (x-axis) CIEs at Walvis Ridge versus paleosol carbonate (y-

773　　　　axis) CIEs in the Bighorn Basin, Wyoming (USA). Trendlines are forced through

774　　　　the origin. Note the apparent reduced CIE for the PETM in paleosol carbonate if

775　　　　extrapolation is used of the trendline through ETM2, H2, I1, and I2.

Figure 5. Carbon isotope excursions (CIEs) for the PETM, ETM2, H2, I1, and I2 events in the early Eocene compared between paleosol carbonate (y-axis) CIEs in the Bighorn Basin, Wyoming (USA) and measured and modeled plant CIE for two extreme initial pCO$_2$ scenarios. The plant CIE for the PETM is measured (Smith et al. 2007), those of the younger four hyperthermals modeled (see text for explanation). Note that the trendlines for both extreme pCO2 scenarios do not fit the measured CIEs in plant and pedogenic carbonate for the PETM.
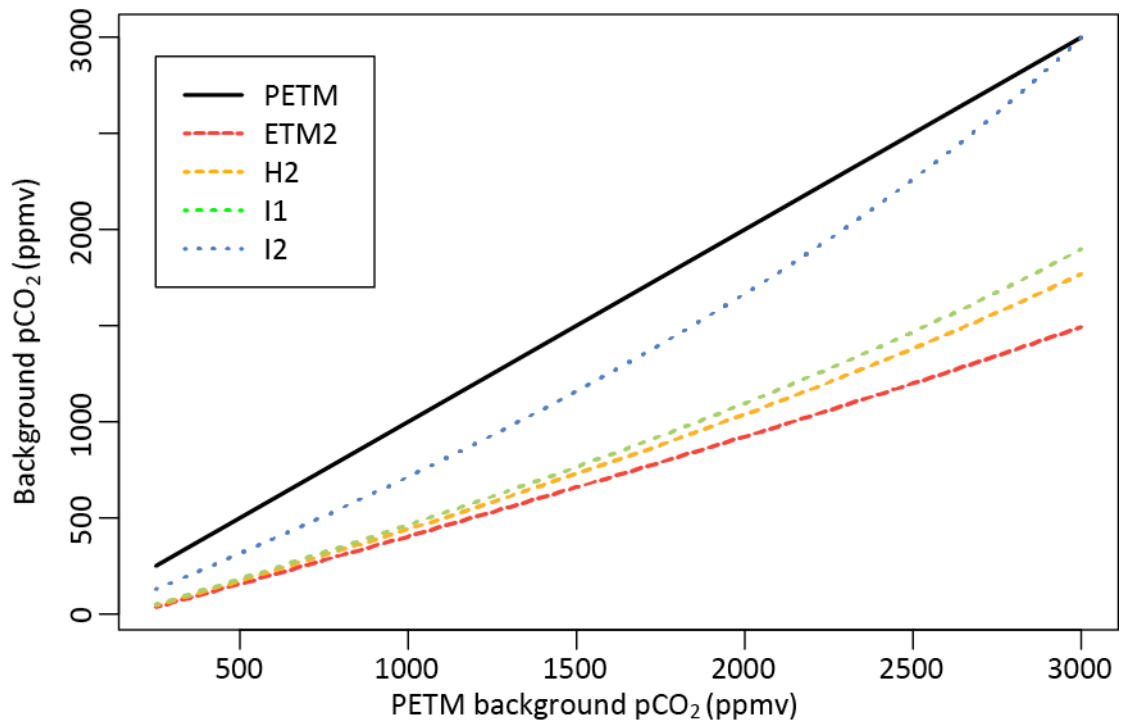
Figure 6. Model results of pCO_2 scenarios for the four younger hyperthermals finding a solution for the non-linear scaling of the soil carbonate CIEs relative to the marine record changes in photosynthetic ^{13}C-discrimination forced by hyperthermal pCO_2 increase over a varying background pCO_2 conditions. A solution is found across the entire range of assumed PETM background pCO_2 conditions. Note that this requires a >50% decrease in background pCO_2 for most of the post-PETM hyperthermals.